Stochastic Modeling of Nonlinear Circuits via SPICE-Compatible Spectral Equivalents

Stochastic Modeling of Nonlinear Circuits via SPICE-Compatible Spectral Equivalents

Paolo Manfredi, DriesVandeGinste, Daniël De Zutter, a n d
Flavio G. Canavero

***Abstract*—This paper presents a systematic approach for the statistical simulation of nonlinear networks with uncertain circuit elements. The proposed technique is based on spectral expansions of the elements' constitutive equations (I–V characteristics) into polynomial chaos series and applies to arbitrary circuit components, both linear and nonlinear. By application of a stochastic Galerkin method, the stochastic problem is cast in terms of an augmented set of deterministic constitutive equations relating the voltage and current spectral coefficients. These new equations are given a circuit interpretation in terms of equivalent models that can be readily implemented in SPICE-type simulators, as such allowing to take full advantage of existing algorithms and available built-in models for complex devices, like diodes and MOSFETs. The pertinent statistical information of the entire nonlinear network is retrieved via a single simulation. This approach is both accurate and efficient with respect to traditional techniques, such as Monte Carlo sampling. Application examples, including the analysis of a diode rectifier, a CMOS logic gate and a low-noise amplifier, validate the methodology and conclude the paper.**

***Index Terms*—Circuit design, circuit simulation, nonlinear circuits, polynomial chaos, SPICE, statistical analysis, uncertainty.**

I. Introduction

THE increasing miniaturization of electronic equipment is amplifying the impact of tolerances and uncertainties on circuit performance. The variability has several sources, ranging from the manufacturing process to temperature fluctuations and aging, and requires the electrical response to be addressed from a statistical standpoint. A common practice to handle this inherent randomness in circuit simulators is to use Monte Carlo [1] or similar sampling-based methods. A sufficiently large set of different scenarios is generated according to the statistical properties of the random parameters and simulated to collect samples of the output response. Despite its simplicity, the main drawback lies in the large number of instances that must be considered, thus often making the computational time prohibitive. To speed-up the design phase, engineers have been seeking for more efficient techniques (e.g., [2]).

Great attention has been recently attracted by the framework of the polynomial chaos (PC) theory [3]. Leveraging PC, random quantities and their governing equations are expanded into series of orthogonal polynomials, suitably chosen depending on the probability distribution [4]. The unknown expansion coefficients are computed via the solution of an augmented system of equations, constructed using a stochastic Galerkin method (SGM). Pertinent statistical information is then readily obtained from these coefficients.

On the one hand, the technique has been used in [5] and [6] to analyze linear RLC networks. A more systematic and circuit-oriented approach was proposed in [7], where equivalent circuit models were proposed to model uncertainties in lumped linear electrical devices. The approach was later implemented in a customized circuit analysis tool having a (limited) capability of handling also nonlinear components [8]. However, an important limitation is that device nonlinearities are handled using either small-signal, linearized equivalent models, or approximate Taylor expansions. Alternative and noteworthy approaches to handle more general nonlinear circuits have been recently proposed in [9], but limited to Gaussian variability only, and [10], [11]. Nevertheless, one of the main limitations in [8]–[11] is that an ad-hoc software, in which customized library models must be re-developed for each device, is required, rather than relying on available and standard circuit solvers. As modern simulators offer well-consolidated algorithms and hundreds of sophisticated device models, compatibility with commercial software is a very desirable requirement for circuit designers.

On the other hand, the authors of this paper proposed a PC-based modeling strategy for the statistical assessment of stochastic distributed networks in standard SPICE-type design environments [12]. Nonetheless, the methodology presented in [12] focuses exclusively on the variability provided by transmission-line elements with random properties, while lacking the inclusion of random lumped elements as well as of nonlinear components. The present paper covers this gap by outlining a very general framework for stochastic circuit simulation, consisting of random linear and nonlinear components. The latter include elements with user-defined I–V characteristic or built-in device models, like those for diodes and MOSFETs available in many SPICE-type simulators. It is important to stress that the proposed modeling technique is fully compatible with standard and commercially available circuit solvers.

This paper is organized as follows. Section II outlines the basic principles of PC; Section III introduces the modeling of random linear circuit elements; Section IV describes the modeling of nonlinear devices; Section V outlines the general

P. Manfredi and F. G. Canavero are with the EMC Group, Department of Electronics and Telecommunications, Politecnico di Torino, 10129 Torino, Italy (e-mail: paolo.manfredi@polito.it; flavio.canavero@polito.it).

D. Vande Ginste and D. De Zutter are with the Electromagnetics Group, Department of Information Technology, Ghent University, 9000 Gent, Belgium (e-mail: dries.vandeginste@ugent.be; daniel.dezutter@ugent.be).

procedure for the PC-based simulation of stochastic networks; in Section VI, the proposed approach is illustrated and validated by means of application examples, whereas its efficiency is assessed in Section VII; finally, conclusions are drawn in Section VIII.

II. Polynomial Chaos Overview

In an electrical network where some elements are stochastic, voltages and currents also become stochastic. The underlying idea for the simulation of such a stochastic network is to expand voltages and currents into the spectral PC series [12], i.e.,

$$v(t,\boldsymbol{\xi}) \approx \sum_{k=0}^{P} v_k(t)\varphi_k(\boldsymbol{\xi}), \quad i(t,\boldsymbol{\xi}) \approx \sum_{k=0}^{P} i_k(t)\varphi_k(\boldsymbol{\xi}) \qquad (1)$$

where $\boldsymbol{\xi} = [\xi_1, \ldots, \xi_d]$ is a vector collecting the independent and normalized random variables (RVs) parameterizing all the variations (e.g., manufacturing tolerances and/or temperature fluctuations).[1] Furthermore, $v_k(t)$ and $i_k(t)$ are deterministic voltage and current coefficients to be determined. Finally, $\{\varphi_k\}_{k=0}^{P}$ forms a basis of multivariate polynomial functions that are *orthonormal* with respect to the following inner product:

$$\langle f, g\rangle = \int_{\mathbb{R}^d} f(\boldsymbol{\xi})g(\boldsymbol{\xi})w(\boldsymbol{\xi})d\boldsymbol{\xi} \qquad (2)$$

$w(\boldsymbol{\xi})$ being the joint probability distribution of $\boldsymbol{\xi}$.

According to the Wiener-Askey scheme, the polynomials satisfying the orthogonality condition $\langle\varphi_k, \varphi_j\rangle = 0$, $k \neq j$, for $d = 1$ and standard distributions $w(\xi)$ are known and correspond, e.g., to Hermite polynomials for Gaussian RVs ($w = (1/\sqrt{2\pi})\mathrm{e}^{-\xi^2/2}$), Legendre polynomials for uniform RVs ($w = 1/2$, $|\xi| \leq 1$), etc. [4], and ad-hoc polynomials can be devised for nonstandard distributions. It is important to point out, however, that in general $\langle\varphi_k, \varphi_k\rangle \neq 1$, i.e., such polynomials are not orthonormal. In order to preserve symmetry and reciprocity of the models, a *normalized* (i.e., rescaled) version of such polynomials, rendering $\langle\varphi_k, \varphi_j\rangle = \delta_{kj}$ (Kronecker's delta), must be adopted [13]. When $d > 1$, the multivariate polynomials are built as product combinations of univariate ones, in order to preserve their orthonormality [3].

The expansions (1) are truncated to a maximum *total degree* p of the multivariate polynomials φ_k, so that the total number of terms is $P + 1 = (p + d)!/(p!d!)$. As shown, e.g., in [12], for a broad class of problems, choosing $p = 2$ generally provides satisfactory modeling accuracy.

The main advantage of the PC representation (1) is that the spectral voltages and currents are deterministic, the randomness being confined into the polynomials. Thanks to the orthogonality properties, the first two statistical moments of the circuit variables are readily obtained as $\mathrm{E}\{v(t,\boldsymbol{\xi})\} = v_0(t)$ ($\mathrm{E}\{i(t,\boldsymbol{\xi})\} = i_0(t)$) and $\mathrm{Var}\{v(t,\boldsymbol{\xi})\} = \sum_{k=1}^{P} v_k^2(t)$ ($\mathrm{Var}\{i(t,\boldsymbol{\xi})\} = \sum_{k=1}^{P} i_k^2(t)$) [3]. Higher order moments as well as probability density functions (PDFs) are obtained by randomly sampling (1) in accordance with the distribution of $\boldsymbol{\xi}$. This postprocessing procedure is very fast because (1) is merely a polynomial function.

[1] Any random parameter x, for example a resistor value, temperature, or a nonlinear device model parameter, can be parameterized as $x = \bar{x} + \Delta x\xi_i$, with $\bar{x}$ its mean and $\Delta x\xi_i$ its deviation from the mean. The distribution of this deviation is defined by the probability density function of ξ_i.

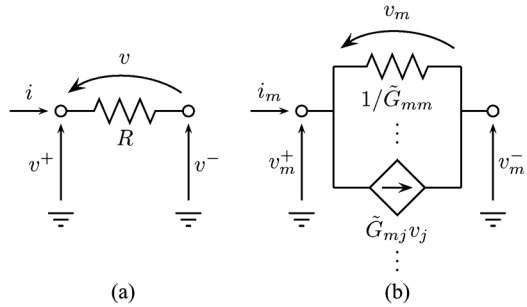

Fig. 1. Resistor element (a) and corresponding equivalent circuit for the mth spectral coefficients (b).

III. Modeling of Linear Elements

As discussed in the previous section, the statistical information on the circuit response is readily obtained, provided that the spectral coefficients $v_k(t)$ and $i_k(t)$ of the node voltages and branch currents are known. In order to avoid repeated and time-consuming simulations of the stochastic network, in [12] pertinent equivalent circuit models are created, connected and simulated in a SPICE-type tool to retrieve $v_k(t)$ and $i_k(t)$.

Unfortunately, in [12], only (multiconductor) transmission lines with random cross-sectional properties in combination with deterministic linear lumped elements are discussed. In this paper, a far more general framework is outlined, in which both linear and nonlinear elements, possibly subject to variability themselves, can be included. The discussion starts from the basic linear elements, i.e., resistors, capacitors, and inductors. The modeling of nonlinear devices is discussed in the next section.

A. Resistors

The current-voltage relationship of a resistor, shown in Fig. 1(a), is governed by Ohm's law

$$i(t) = G\left(v^+(t) - v^-(t)\right) = Gv(t) \qquad (3)$$

with $G = 1/R$ and $v^{\pm}$ being the node voltages of the positive and negative terminals. If the resistance R is random, e.g., due to manufacturing tolerances or temperature variations, its conductance can be expressed with a PC expansion analogous to (1), i.e.,

$$G(\boldsymbol{\xi}) = \frac{1}{R(\boldsymbol{\xi})} \approx \sum_{k=0}^{P} G_k\varphi_k(\boldsymbol{\xi}) \qquad (4)$$

and, hence, the voltage and current in (3) become random themselves. Given the orthonormality of the polynomials, the coefficients G_k are found as $G_k = \langle G, \varphi_k\rangle = \int_{\mathbb{R}^d}(1/R(\boldsymbol{\xi}))\varphi_k(\boldsymbol{\xi})w(\boldsymbol{\xi})d\boldsymbol{\xi}$. Introducing (4) and (1) into (3) yields

$$\sum_{k=0}^{P} i_k(t)\varphi_k(\boldsymbol{\xi}) = \sum_{k=0}^{P}\sum_{j=0}^{P} G_k v_j(t)\varphi_k(\boldsymbol{\xi})\varphi_j(\boldsymbol{\xi}). \qquad (5)$$

Application of a SGM, i.e., multiplying the left- and right-hand sides of (5) by $\varphi_m(\boldsymbol{\xi})$ and integrating them using the inner product (2)

$$\left\langle \sum_{k=0}^{P} i_k(t)\varphi_k, \varphi_m \right\rangle = \left\langle \sum_{k=0}^{P}\sum_{j=0}^{P} G_k v_j(t)\varphi_k\varphi_j, \varphi_m \right\rangle \quad (6)$$

leads to

$$i_m(t) = \sum_{j=0}^{P} \tilde{G}_{mj} v_j(t) = \sum_{j=0}^{P} \tilde{G}_{mj}\left(v_j^+(t) - v_j^-(t)\right) \quad (7)$$

where we used the orthogonality condition and defined

$$\tilde{G}_{mj} = \sum_{k=0}^{P} G_k \alpha_{kjm} \quad (8)$$

with

$$\alpha_{kjm} = \langle \varphi_k\varphi_j, \varphi_m\rangle = \int_{\mathbb{R}^d} \varphi_k(\boldsymbol{\xi})\varphi_j(\boldsymbol{\xi})\varphi_m(\boldsymbol{\xi})w(\boldsymbol{\xi})d\boldsymbol{\xi}. \quad (9)$$

For standard polynomial classes, the result of the above integral (9) is analytically available.

It is worthwhile noting that (7) is now a *deterministic* equation relating the mth spectral current coefficient to all the spectral voltage coefficients. By repeating the above procedure for m going from 0 to P, a set of $P+1$ deterministic equations is obtained. This result corresponds to the sought-for constitutive relationships linking all the spectral voltage and current coefficients. This complete system of equations can be cast in matrix form as

$$\tilde{\mathbf{i}}(t) = \tilde{\mathbf{G}}\tilde{\mathbf{v}}(t) = \tilde{\mathbf{G}}\left(\tilde{\mathbf{v}}^+(t) - \tilde{\mathbf{v}}^-(t)\right) \quad (10)$$

with $\tilde{\mathbf{i}}(t) = [i_0(t), \ldots, i_P(t)]^T$, $\tilde{\mathbf{v}}^{(\pm)}(t) = [v_0^{(\pm)}(t), \ldots, v_P^{(\pm)}(t)]^T$, and the entries of matrix $\tilde{\mathbf{G}}$ are given in (8).

Equations like (7) can be implemented in any circuit solver using the equivalent circuit illustrated in Fig. 1(b). In fact, according to (7), the total current in the mth branch is the sum of $P+1$ contributions. The term for $j = m$, i.e., $\tilde{G}_{mm}$, still describes a resistor, while the terms $\tilde{G}_{mj}$ are transconductances providing coupling among the other spectral branches and they are implemented by means of parallel voltage-dependent current sources, in accordance with the Kirchhoff current law (KCL).

B. Capacitors

The constitutive equation of a capacitor, shown in Fig. 2(a), is

$$i(t) = C\frac{d}{dt}\left(v^+(t) - v^-(t)\right) = C\frac{d}{dt}v(t). \quad (11)$$

Application of the SGM leads to

$$i_m(t) = \sum_{j=0}^{P} \tilde{C}_{mj}\frac{d}{dt}v_j(t), \quad \forall m = 0, \ldots, P \quad (12)$$

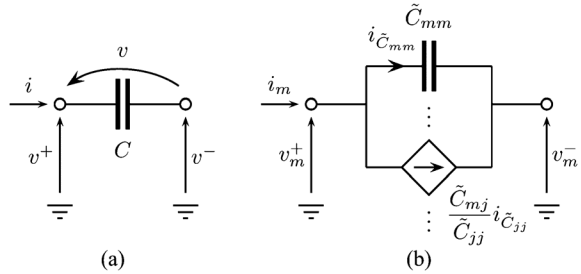

Fig. 2. Capacitor element (a) and corresponding equivalent circuit for the mth spectral coefficients (b).

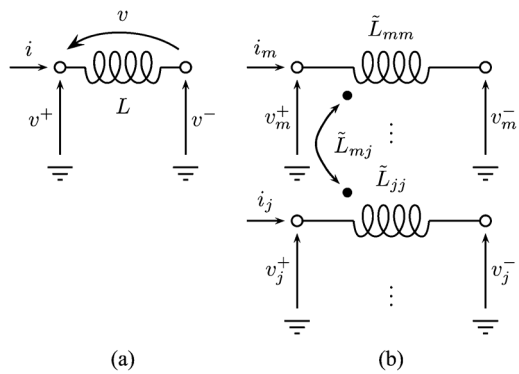

Fig. 3. Inductor element (a) and corresponding equivalent circuit for the mth spectral coefficients (b).

with $\tilde{C}_{mj} = \sum_{k=0}^{P} C_k\alpha_{kjm}$. In matrix form, $\forall m$, this becomes

$$\tilde{\mathbf{i}}(t) = \tilde{\mathbf{C}}\frac{d}{dt}\tilde{\mathbf{v}}(t) = \tilde{\mathbf{C}}\frac{d}{dt}\left(\tilde{\mathbf{v}}^+(t) - \tilde{\mathbf{v}}^-(t)\right). \quad (13)$$

The equivalent circuit for the mth spectral (12) is shown in Fig. 2(b). Whereas the contribution for $j = m$ still corresponds to a capacitance $\tilde{C}_{mm}$, the coupling terms $\tilde{C}_{mj}$ are added via current-dependent current sources transferring the effects of time derivatives in (12).

C. Inductors

The behavior of an inductor, shown in Fig. 3(a), is governed by the following equation:

$$v^+(t) - v^-(t) = v(t) = L\frac{d}{dt}i(t). \quad (14)$$

The same SGM-based procedure used for resistors and capacitors leads to

$$v_m(t) = v_m^+(t) - v_m^-(t) = \sum_{j=0}^{P} \tilde{L}_{mj}\frac{d}{dt}i_j(t) \quad (15)$$

or, in matrix form $\forall m$,

$$\tilde{\mathbf{v}}(t) = \tilde{\mathbf{v}}^+(t) - \tilde{\mathbf{v}}_m^-(t) = \tilde{\mathbf{L}}\frac{d}{dt}\tilde{\mathbf{i}}(t) \quad (16)$$

where once again $\tilde{L}_{mj} = \sum_{k=0}^{P} L_k\alpha_{kjm}$. The mth spectral (15) corresponds to the voltage across an inductor with multiple couplings to the other spectral circuits. Therefore, the pertinent equivalent circuit is illustrated in Fig. 3(b).

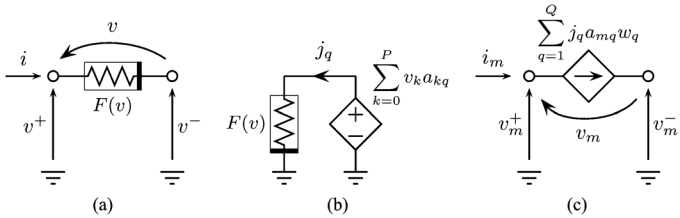

Fig. 4. Nonlinear conductance (a), illustration of the corresponding qth companion cell (b), and equivalent circuit for the mth spectral coefficients (c).

The equivalent circuits in Figs. 1–3 are readily implemented in any, e.g., SPICE-type, circuit simulator. For each random component, the corresponding spectral circuits are generated in an automated fashion after calculation of the pertinent matrix $\tilde{\mathbf{G}}$, $\tilde{\mathbf{C}}$ or $\tilde{\mathbf{L}}$, and included as a subcircuit.

It is important to remark that the augmented constitutive equations derived so far for resistors (10), capacitors (13), and inductors (16), were proven to describe passive models, independently of their specific circuit implementation. This is due to the positive-definitess of their corresponding matrices [14]. So, adopting the new implementation as proposed in the present paper, guarantees stability during, e.g., transient simulations.

IV. Modeling of Nonlinear Elements

When the governing equations are nonlinear, the derivation of the constitutive equations relating the voltage and current coefficients is hindered by the fact that, in general, no closed-form expression exists for the integrals appearing in the SGM. A novel, efficient, and SPICE-compatible modeling strategy to tackle this issue is outlined in this section, starting from the case of two-terminal nonlinear elements having a deterministic I–V characteristic. The formulation is later extended to three-terminal elements (transistors) as well as to nonlinear elements with randomness in their characteristic.

A. Deterministic Two-Terminal Devices

Let us consider the case of a generic nonlinear conductance [Fig. 4(a)]

$$i(t) = F\left(v^+(t) - v^-(t)\right) = F\left(v(t)\right). \tag{17}$$

Substitution of the expansions (1) into (17) yields

$$\sum_{k=0}^{P} i_k(t)\varphi_k(\boldsymbol{\xi}) = F\left(\sum_{k=0}^{P} v_k(t)\varphi_k(\boldsymbol{\xi})\right). \tag{18}$$

Application of the SGM produces, $\forall m = 0, \ldots, P$,

$$i_m(t) = \int_{\mathbb{R}^d} F\left(\sum_{k=0}^{P} v_k(t)\varphi_k(\boldsymbol{\xi})\right)\varphi_m(\boldsymbol{\xi})w(\boldsymbol{\xi})d\boldsymbol{\xi}. \tag{19}$$

As anticipated, in general the integral in the right-hand side cannot be resolved in closed form, except when the nonlinear function $F(\cdot)$ is of the polynomial type [15].

When the function is not polynomial, but for example an exponential diode equation, a very general, approximate formulation to solve the issue has been presented in [16]. The integral in (19) is discretized by means of a quadrature rule $\forall m = 0, \ldots, P$

$$\begin{aligned} i_m(t) &\approx \sum_{q=1}^{Q} F\left(\sum_{k=0}^{P} v_k(t)\varphi_k(\boldsymbol{\xi}_q)\right)\varphi_m(\boldsymbol{\xi}_q)w_q \\ &= \sum_{q=1}^{Q} j_q\left(t, v_0(t), \ldots, v_P(t)\right) a_{mq} w_q \end{aligned} \tag{20}$$

where we introduced the notation $a_{mq} = \varphi_m(\boldsymbol{\xi}_q)$ and

$$j_q\left(t, v_0(t), \ldots, v_P(t)\right) = F\left(\sum_{k=0}^{P} v_k(t) a_{kq}\right) \tag{21}$$

with $a_{kq} = \varphi_k(\boldsymbol{\xi}_q)$. In (20), Q is the number of quadrature points, whereas $\boldsymbol{\xi}_q$ are predefined multivariate samples of the RVs $\boldsymbol{\xi}$ and w_q are the corresponding weights, both depending on the quadrature rule. As such, a_{mq} and a_{kq} are merely (precomputable) coefficients, thus rendering (20) a deterministic equation. Such an equation involves linear combinations of all the voltage spectral coefficients in the argument of the nonlinear function, as well as linear combinations of the nonlinear currents. As shown in the application examples, by using proper Gaussian quadrature rules [17], a very good modeling accuracy can be achieved with a low number of quadrature points. Other quadrature rules may of course be used. However, this would not modify the stamp and the circuit interpretation of (20) that is presented below.

When the nonlinear I–V characteristic is known in analytical form, like for example the Schottky diode equation $i(t) = F(v(t)) = I_s(\exp(v(t)/V_T) - 1)$, (20) could be implemented using behavioral dependent sources available in advanced circuit simulators. Nonetheless, we propose a more efficient and elegant circuit implementation of (20), which is also valid for user-defined and library elements with non-analytical characteristics. This implementation is inspired by the observation that, for every m, the summation over q always involves the same nonlinear terms j_q (21). Therefore, the idea is to introduce an auxiliary, companion circuit cell responsible for the sampling of these nonlinear currents, as illustrated in Fig. 4(b). A voltage-dependent voltage source is used to linearly combine the spectral voltage coefficients appearing in the argument of the nonlinear function. The nonlinear element with the pertinent I–V characteristic $F(v(t))$ guarantees that the current j_q flows in the companion circuit. In total, Q such companion cells are defined and the Q nonlinear currents j_q are linearly combined in the main circuit by means of current-dependent current sources, as shown in Fig. 4(c).

It is important to note that, according to this implementation, the overall circuit model involves the same type of nonlinearity $F(v)$ as the original circuit. This makes this implementation very efficient, despite the additional number of auxiliary nodes required by the companion cells. Moreover, as stated above, the nonlinear element can now be *any* user-defined device or library element (e.g., a diode) available in the solver, as there is no more need to have an explicit analytical I–V characteristic.

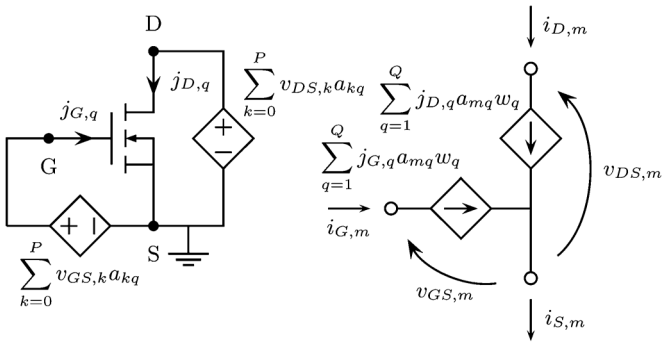

Fig. 5. Illustration of the qth companion cell (left) and the equivalent circuit for the mth spectral coefficients (right) of a nonlinear three-terminal device.

B. Three-Terminal Devices

Reasoning along the same lines, three-terminal devices, like transistors, can also be dealt with. The structure of the companion cell and the spectral equivalent model are illustrated in Fig. 5 for a MOSFET. In this case, two voltage sources are required in the companion cell to linearly combine the input and output voltages, i.e., the gate-source and drain-source voltages, respectively. The resulting nonlinear gate and drain currents are then linearly combined in the spectral equivalent circuit by means of two dependent current sources. The current in the source terminal is determined by the KCL.

C. Stochastic Nonlinear Devices

If the nonlinear elements also exhibit variability, their characteristic inherently depends on the random vector $\boldsymbol{\xi}$, i.e., $F = F(v(t), \boldsymbol{\xi})$. As the integral in (19) is already sampled at the quadrature points $\boldsymbol{\xi}_q$, now the nonlinear currents (21) become

$$j_q\left(t, v_0(t), \ldots, v_P(t)\right) = F|_{\boldsymbol{\xi}_q}\left(\sum_{k=0}^{P} v_k(t)a_{kq}\right) \tag{22}$$

where $F|_{\boldsymbol{\xi}_q} = F(v(t), \boldsymbol{\xi}_q)$ denotes the sampled nonlinear characteristic. Again, the nonlinear circuit component may be simulated using the built-in device models. It suffices to define companion cells for each $\boldsymbol{\xi}_q$. This reasoning applies to both two- and three-terminal devices.

V. Simulation Procedure

Given the equivalent spectral circuit models introduced in the previous sections, the strategy for the PC-based simulation of a stochastic electrical network is as follows.

1) Assume node voltages and branch currents to be expanded according to (1).
2) For each component in the original network, build the $P+1$ spectral models as described in Sections III and IV.
3) Create a new augmented network, by associating a node to each voltage spectral coefficient, and properly connect these nodes in accordance with the original circuit topology.
4) Simulate the obtained network to calculate the sought-for spectral voltage and current coefficients of the stochastic network, coinciding with the deterministic voltages and currents of the augmented network. Although augmented, performing a single circuit simulation of this deterministic network is often much faster than running a large number of Monte Carlo simulations of the original stochastic network, as will be shown in the next section.

The above procedure can be easily automated and the inclusion of independent sources in the modeling is straightforward. For a deterministic voltage source $e(t)$, we get $v(t) = v^+(t) - v^-(t) = e(t)$, and application of the SGM produces

$$v_m(t) = v_m^+(t) - v_m^-(t) = \begin{cases} e(t) & m = 0 \\ 0 & \forall m \neq 0. \end{cases} \tag{23}$$

A similar reasoning equivalently applies to independent current sources. Although not often done in practice, stochastic sources can be modeled as well.

The outlined procedure is illustrated in Fig. 6, where a rectifier circuit with three nodes, namely A, B, and C, is considered. For the sake of clarity, a PC expansion with only $P + 1 = 2$ terms is assumed. Two spectral networks are therefore present. Moreover, a number $Q = 2$ of companion cells are considered for the spectral model of the diode. The labels $D|_{\boldsymbol{\xi}_1}$ and $D|_{\boldsymbol{\xi}_2}$ attached to the diodes indicate that the random parameters of the diode model D are sampled at the two quadrature points $\boldsymbol{\xi}_1$ and $\boldsymbol{\xi}_2$. Of course, the null excitation in Fig. 6, evolving from (23), could have been replaced by a short circuit. A netlist example describing the circuit of Fig. 6 in HSPICE is given in the Appendix.

VI. Validation and Numerical Results

This section discusses three validation and application examples, illustrating the accuracy, efficiency, and appositeness of the proposed simulation methodology. All the simulations are carried out with HSPICE [18] on an ASUS U30S laptop with an Intel Core i3-2330M, CPU running at 2.20 GHz and 4 GB of RAM. The complete HSPICE augmented netlists for these examples are available on www.emc.polito.it/TCASI2014/netlists.

A. Full-Bridge Diode Rectifier

The first example considers the full-bridge diode rectifier shown in Fig. 7 [8]. The input signal v_{in} is a sinusoidal voltage source with a peak amplitude of 5 V and a frequency of 60 Hz. The load resistance and capacitance values are $R = 1$ kΩ and $C = 1$ mF, respectively. For the diodes, a standard SPICE model is used, having a series resistance of 1 Ω, a junction capacitance of 2 pF and a saturation current of 50 fA. The variability is provided by the operating temperature of the device, which uniformly varies in the range [0,120]°C. The temperature fluctuation affects both the diodes and the RC load. For the latter, temperature coefficients of $\alpha_R = 1500$ ppm/°C and $\alpha_C = -750$ ppm/°C are assumed for the resistor and the capacitor, respectively.

Fig. 8 shows the result of the stochastic simulation. The gray lines are a subset of 100 Monte Carlo samples providing a qualitative idea of the fluctuation of the rectifier output voltage v_{out} due to temperature variations. The blue lines indicate the average response as well as the 0.135% and 99.865% quantiles. These curves are estimated from 10 000 Monte Carlo samples. Finally, the red markers denote the same statistical information obtained via the PC-based simulation of the deterministic spectral circuit, constructed considering $p = 2$. For the modeling of the diodes, a Gauss–Legendre quadrature with $Q = 3$ was considered. Excellent accuracy is established.

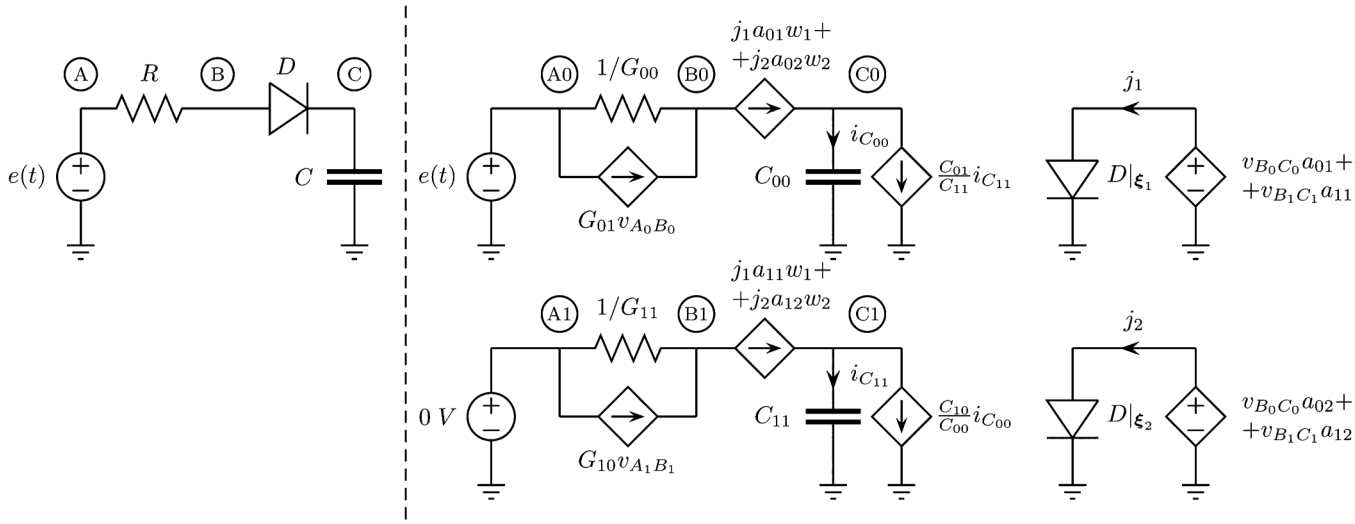

Fig. 6. Illustrative example: rectifier circuit. (Left panel) Original stochastic network. (Rright panel) Spectral circuits for $m = 0$ and $m = 1$ and pertinent companion cells for $q = 1$ and $q = 2$.

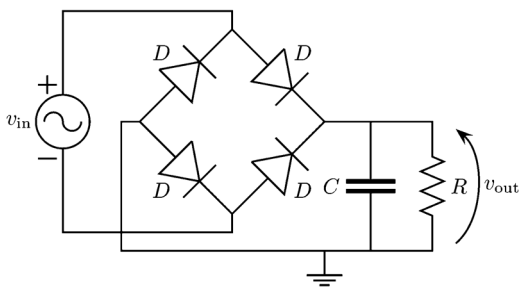

Fig. 7. Circuit schematic of the full-bridge diode rectifier.

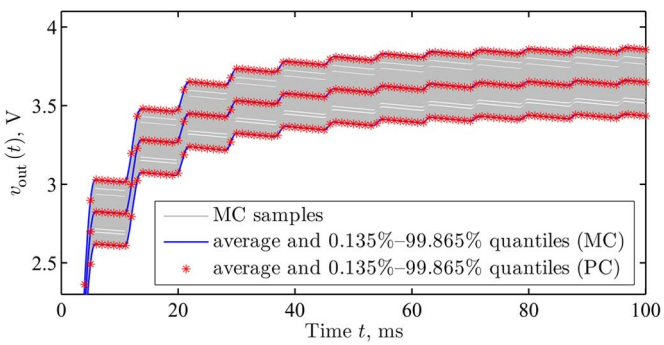

Fig. 8. Output voltage v_{out} of the rectifier in Fig. 7. (Gray lines) Subset of 100 samples from Monte Carlo simulation. (Blue lines) Average response and 0.135%–99.865% quantiles estimated with Monte Carlo analysis. The red asterisks indicate the same statistical information obtained from the PC expansion.

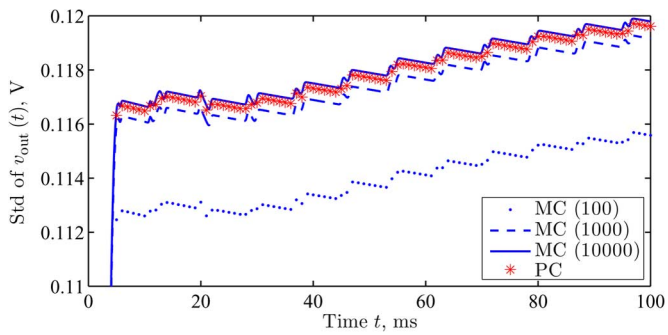

Fig. 9. Standard deviation of the rectifier output. (Blue curves) Results from Monte Carlo simulations with increasing number of samples. (Red asterisks) Result from the PC-based approach.

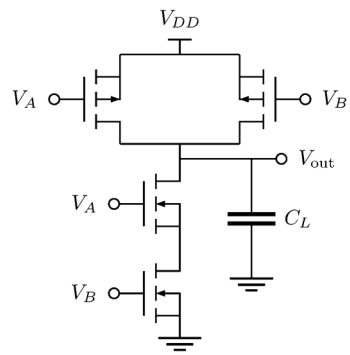

Fig. 10. Schematic of a two-input NAND gate in CMOS technology.

To assess the convergence of the Monte Carlo analysis, Fig. 9 shows the standard deviation of the rectifier output computed both from the PC coefficients and with an increasing number of Monte Carlo runs, i.e., 100, 1000, and 10 000. The relative accuracy between the PC curve and the Monte Carlo estimation with 10 000 samples is on the order of 0.1%.

B. CMOS NAND Gate

The second application example concerns a two-input NAND gate in CMOS technology, whose schematic is depicted in Fig. 10. The load capacitance C_L models the input gate capacitance of the following stage and is considered as a Gaussian random variable with a mean value of 10 pF and a relative standard deviation of 10%. For the n- and p-MOSFETs, a SPICE level-2 model is considered. Among the many parameters, a gate length of 1.2 μm, an oxide thickness of 20 nm, and gate-drain and gate-source capacitances of 0.43 nF are assumed. Finally, the power supply voltage is $V_{DD} = 5$ V.

Fig. 11 shows the response of the logic gate for time varying inputs V_A (solid black line) and V_B (dashed gray line). The gray

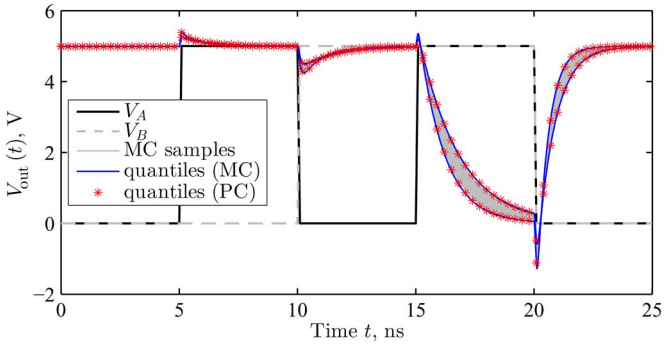

Fig. 11. Simulation result of the NAND gate in Fig. 10. (Solid black line and dashed gray line) Input gate voltages. (Gray area) Subset of 100 samples of the output voltage from Monte Carlo simulation. (Blue lines and red asterisks) 0.135% and 99.865% quantiles of the output estimated with Monte Carlo and PC, respectively.

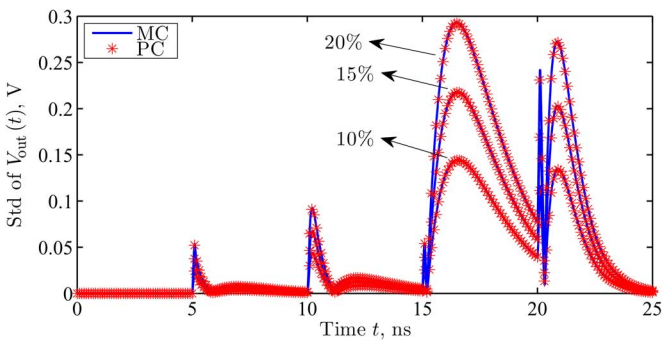

Fig. 12. Standard deviation of the NAND gate output voltage for increasing capacitance variations. (Blue curves) Results from Monte Carlo simulation. (Red asterisks) Results from the PC-based analysis.

area shows the fluctuation of the response due to the load variability. The blue lines indicate the 0.135%–99.865% quantiles estimated after 10 000 Monte Carlo runs, whilst the red markers show the same quantities obtained from the PC-based circuit simulation. For the latter, we used again $p = 2$ and, for the transistors, a Gauss–Hermite quadrature with $Q = 3$ was adopted. To assess the accuracy when larger variations are considered, a comparison of the standard deviation for different capacitance variations (i.e., 10%, 15%, and 20%) is provided in Fig. 12, revealing excellent agreement in each case.

C. Low-Noise Amplifier

The third example deals with the low-noise amplifier depicted in Fig. 13, taken from the HSPICE manual [18] and made up of three 0.25-μm-process n-MOSFETs. The RF input is a 1-GHz sine wave with a peak amplitude of 1 V. The variability is induced by the process tolerance on the inductors, whose values are considered as two independent Gaussian RVs with means $L_1 = 13$ nH and $L_2 = 0.9$ nH and a relative standard deviation of 5%. The values of the remaining circuit elements are $R_S = 50\ \Omega$, $R_1 = 400\ \Omega$, $R_2 = 255\ \Omega$, $R_3 = 120\ \Omega$, and $V_{\text{bias}} = 1.19$ V. The power supply voltage is $V_{DD} = 2.3$ V and the three MOSFET devices are simulated using accurate level-49 SPICE models. For the PC-based modeling of the MOSFETs, a bivariate Gauss–Hermite quadrature with $Q = 9$ is adopted.

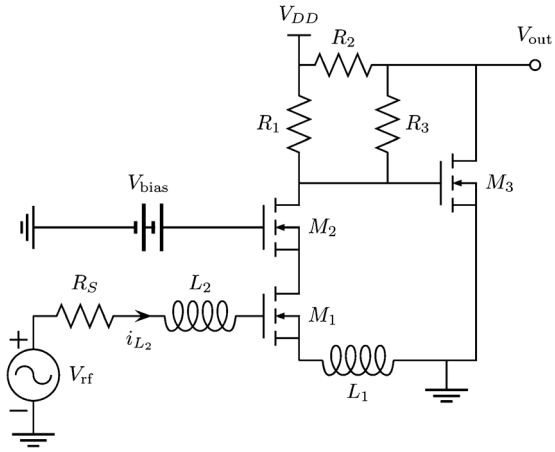

Fig. 13. Circuit schematic of the low-noise amplifier.

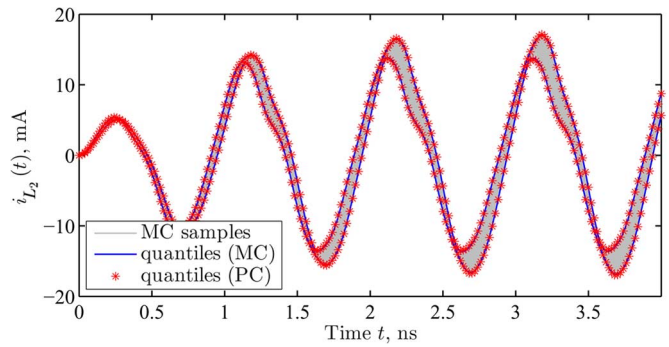

Fig. 14. Current i_{L_2}. (Gray area) Subset of 100 samples from Monte Carlo simulation. (Blue lines and red asterisks) 0.135%–99.865% quantiles of the output estimated with Monte Carlo and PC, respectively.

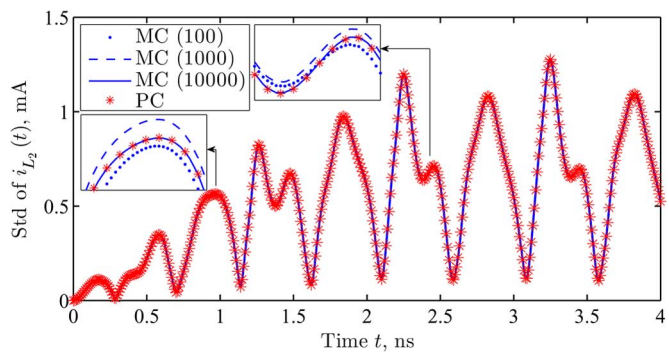

Fig. 15. Standard deviation of i_{L_2}. (Blue curves) Results from Monte Carlo analyses with increasing number of samples. (Red asterisks) Result from the PC-based simulation.

Fig. 14 provides the result of a stochastic simulation of the current i_{L_2} flowing through inductor L_2. Again, the fluctuation of the current due to variability of the inductors is illustrated by means of Monte Carlo samples indicated in gray. The 0.135% and 99.865% quantiles obtained with both Monte Carlo and PC are also shown. A comparison of the standard deviation (see Fig. 15 and, in particular, the two close-ups) shows that, for a comparable accuracy between Monte Carlo and PC, up to 10 000 runs are necessary.

From the PC expansion it is also possible to extract probability distributions. For instance, the PDF of i_{L_2} at $t = 3.12$ ns is given in Fig. 16. The gray bars are the histogram obtained

TABLE I
MAIN FIGURES CHARACTERIZING THE ORIGINAL AND AUGMENTED NETWORKS, AND EFFICIENCY AGAINST MONTE CARLO ANALYSIS

	original network				SGM-based augmented network								
circuit	# nodes	# R/L/C	# nonlin	CPU time	# nodes	# R/L/C	# vcvs	# cccs/vccs	# nonlin	P	Q	CPU time	speed-up
Fig. 7	8	2	4	2520 s	49	6	12	22	12	2	3	1 s	2520×
Fig. 10	14	1	4	10420 s	91	3	24	24	12	2	3	5.2 s	2000×
Fig. 13	10	6	3	2363 s	163	36	54	36	27	5	9	4.6 s	510×

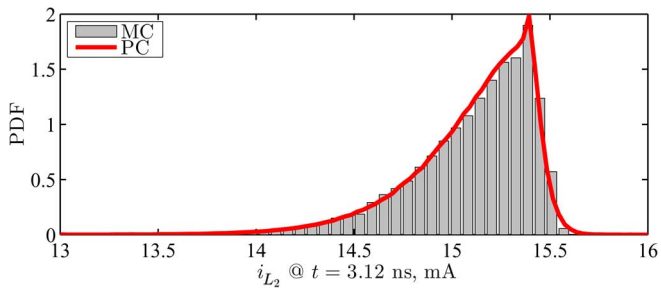

Fig. 16. Probability density function of $i_{L_2}(t)$ at $t = 3.12$ ns. (Gray bars) Estimation of Monte Carlo analysis. (Red line) Result from the PC expansion.

from the Monte Carlo samples, whilst the red line is the PDF evaluated from the PC expansion. Very good accuracy is established. The shape of this PDF differs substantially from a Gaussian distribution, therefore average and standard deviation are not sufficient to fully characterize the statistics of the circuit waveforms.

VII. IMPLEMENTATION DETAILS AND EFFICIENCY ASSESSMENT

As described in Section V, the proposed method requires a single simulation of a netlist with a number of nodes that is in principle $P + 1$ larger than the original stochastic network. However, the modeling of each nonlinear device additionally requires Q companion cells that sample the nonlinear currents (21), as illustrated in Figs. 4 and 5. Although they only include standard elements, the optimal implementation of these companion cells may vary for different simulators. For example, although behavioral sources in HSPICE allow to access circuit currents like j_q, $j_{G,q}$ and $j_{D,q}$ directly, an implementation using 0-V sources to sample such currents turned out to be more efficient, despite the extra nodes it requires. It should also be noted that the inclusion of nonlinear devices might further increase the overall number of nodes, depending on the selected model and corresponding parameters. This makes it difficult to predict the actual size of the original circuit and, consequently, also of the augmented network.

Table I compares network size, number of components and simulation times for the given application examples. In particular, the number of linear (RLC) elements in the augmented network is $P + 1$ larger than the original one, whilst the number of nonlinear elements is Q times larger. Moreover, controlled voltage and current sources (VCVS and CCCS/VCCS, respectively) appear in the augmented network to account for the coupling between the spectral circuits. The CPU time for the original network refers to a 10 000-sample Monte Carlo analysis. Excellent speed-ups, from two to three orders of magnitude, are achieved.

The efficiency of the advocated technique is reduced when the dimensionality in terms of number of RVs d is increased, as this makes both P and Q grow. For large netlists with only a few nonlinear components, the impact of Q is expected to be less significant. Nevertheless, the inclusion of large numbers of RVs in the PC-SGM framework for circuit-level simulations is still under investigation.

VIII. CONCLUSIONS

This paper outlines a systematic procedure for the efficient statistical simulation of general nonlinear circuits in standard SPICE-type design environments. More specifically, it shows that a stochastic circuit containing linear and nonlinear components, including nondeterministic two- and three-terminal devices, is converted into a single deterministic augmented circuit that is readily implemented in SPICE. The proposed procedure is based on the expansion of circuit voltages and currents in terms of PC series, from which the desired statistical information is quickly derived. The PC-based technique provides excellent accuracy and superior efficiency compared to standard sampling-based methods like Monte Carlo.

APPENDIX

For illustration purposes, the HSPICE netlist for the circuit of Fig. 6 is provided below. Nonetheless, the augmented network created by means of the SGM is compatible with any standard commercial circuit solver.

```
$ voltage source
V0 A0 0 tranfun
V1 A1 0 DC = 0

$ resistor model
R00 A0 B0 '1/G00'
G01 A0 B0 A1 B1 G01
G10 A1 B1 A0 B0 G10
R11 A1 B1 '1/G11'

$ diode model
F0 B0 C0 POLY(2)
+ Vsamp1 Vsamp2 0 'a01*w1' 'a02*w2'
F1 B1 C1 POLY(2)
+ Vsamp1 Vsamp2 0 'a11*w1' 'a12*w2'

$ capacitor model
C00 C0 0 C00
G01 C0 0 cur='C01/C11*i(C11)'
G10 C1 0 cur='C10/C00*i(C00)'
C11 C1 0 C11
```

```
$ companion cell #1
E1 X1 0 POLY(2) B0 C0 B1 C1 0 a01 a11
Vsamp1 X1 Y1 DC = 0
D1 Y1 0 diode_model $ use params for \xi_1

$ companion cell #2
E2 X2 0 POLY(2) B0 C0 B1 C1 0 a02 a12
Vsamp2 X2 Y2 DC = 0
D2 Y2 0 diode_model $ use params for \xi_2
```

It should be noted that most of the available commercial simulators are based on the modified nodal analysis (MNA) method [19]. However, due to the presence of controlled sources, the way the augmented circuit is handled might not be the most efficient. Other implementations could be obtained by considering nodal analysis (NA)-based approaches [20], [21].

REFERENCES

[1] G. S. Fishman, *Monte Carlo: Concepts, Algorithms, and Applications*. New York, NY, USA: Springer-Verlag, 1996.

[2] A. H. Zaabab, Q.-J. Zhang, and M. Nakhla, "A neural network modeling approach to circuit optimization and statistical design," *IEEE Trans. Microw. Theory. Tech.*, vol. 43, no. 6, pp. 1349–1358, Jun. 1995.

[3] D. Xiu, "Fast numerical methods for stochastic computations: A review," *Commun. Comput. Phys.*, vol. 5, no. 2–4, pp. 242–272, Feb. 2009.

[4] D. Xiu and G. E. Karniadakis, "The Wiener-Askey polynomial chaos for stochastic differential equations," *SIAM J. Sci. Comput.*, vol. 24, no. 2, pp. 619–622, 2002.

[5] S. Vrudhula, J. M. Wang, and P. Ghanta, "Hermite polynomial based interconnect analysis in the presence of process variations," *IEEE Trans. Comput. Aided Design Int. Circ. Syst.*, vol. 25, no. 10, pp. 2001–2011, Oct. 2006.

[6] N. Mi, S. X.-D. Tan, Y. Cai, and X. Hong, "Fast variational analysis of on-chip power grids by stochastic extended Krylov subspace method," *IEEE Trans. Comput. Aided Design Int. Circ. Syst.*, vol. 27, no. 11, pp. 1996–2006, Nov. 2008.

[7] Q. Su and K. Strunz, "Stochastic circuit modelling with Hermite polynomial chaos," *IET Electron. Lett.*, vol. 41, no. 21, pp. 1163–1165, Oct. 2005.

[8] K. Strunz and Q. Su, "Stochastic formulation of SPICE-type electronic circuit simulation using polynomial chaos," *ACM Trans. Model. Comput. Simul.*, vol. 18, no. 4, pp. 15:1–15:23, Sep. 2008.

[9] M. R. Rufuie, E. Gad, M. Nakhla, and R. Achar, "Generalized Hermite polynomial chaos for variability analysis of macromodels embedded in nonlinear circuits," *IEEE Trans. Compon. Packag. Manuf. Techol.*, to be published.

[10] Z. Zhang, T. A. El-Moselhy, I. M. Elfadel, and L. Daniel, "Stochastic testing method for transistor-level uncertainty quantification based on generalized polynomial chaos," *IEEE Trans. Comput.-Aided Des. Integr. Circuits Syst.*, vol. 32, no. 10, pp. 1533–1545, Oct. 2013.

[11] Z. Zhang, T. A. El-Moselhy, P. Maffezzoni, I. M. Elfadel, and L. Daniel, "Efficient uncertainty quantification for the periodic steady state of forced and autonomous circuits," *IEEE Trans. Circuits Syst. II, Exp. Briefs*, vol. 60, no. 10, pp. 687–691, Oct. 2013.

[12] P. Manfredi, D. Vande Ginste, D. De Zutter, and F. G. Canavero, "Uncertainty assessment of lossy and dispersive lines in SPICE-type environments," *IEEE Trans. Compon. Packag. Manuf. Techol.*, vol. 3, no. 7, pp. 1252–1258, Jul. 2013.

[13] P. Manfredi, D. Vande Ginste, D. De Zutter, and F. G. Canavero, "Improved polynomial chaos discretization schemes to integrate interconnects into design environments," *IEEE Microw. Wireless Compon. Lett.*, vol. 23, no. 3, pp. 116–118, Mar. 2013.

[14] P. Manfredi, D. Vande Ginste, D. De Zutter, and F. G. Canavero, "On the passivity of polynomial chaos-based augmented models for stochastic circuits," *IEEE Trans. Circuits Syst. I, Reg. Papers*, vol. 60, no. 11, pp. 2998–3007, Nov. 2013.

[15] P. Manfredi, A. Biondi, D. Vande Ginste, D. De Zutter, and F. G. Canavero, "SPICE-based statistical assessment of interconnects terminated by nonlinear loads with polynomial characteristics," in *Proc. IEEE 22th Conf. Elect. Perform. Electron. Packag. Syst.*, San Jose, CA, USA, Oct. 2013, pp. 99–102.

[16] A. Biondi, D. Vande Ginste, D. De Zutter, P. Manfredi, and F. G. Canavero, "Variability analysis of interconnects terminated by general nonlinear loads," *IEEE Trans. Compon. Packag. Manuf. Techol.*, vol. 3, no. 7, pp. 1244–1251, Jul. 2013.

[17] G. H. Golub and J. H. Welsch, "Calculation of Gauss quadrature rules," *Math. Computa.*, vol. 23, pp. 221–230, 1969.

[18] *"HSPICE User Guide: Signal Integrity,"* ver. B-2008.09, Synopsys, Inc., Mountain View, CA, USA, Sep. 2008.

[19] C.-W. Ho, A. Ruehli, and P. Brennan, "The modified nodal approach to network analysis," *IEEE Trans. Circuits Syst.*, vol. 22, no. 6, pp. 504–509, Jun. 1975.

[20] C. Sánchez-López, R. Ochoa-Montiel, A. Ruiz-Pastor, and B. M. González-Contreras, "Symbolic nodal analysis of fully-differential analog circuits," in *Proc. 4th IEEE Int. Latin Amer. Symp. Circuits Syst.*, Cusco, Peru, Feb.–Mar. 2013, pp. 1–4.

[21] C. Sánchez-López, A. Ruiz-Pastor, R. Ochoa-Montiel, and M. A. Carrasco-Aguilar, "Symbolic nodal analysis of analog circuits with modern multiport functional blocks," *Radio Eng.*, vol. 22, no. 2, pp. 518–525, Jun. 2013.